A Breakthrough Propulsion Architecture for Interstellar Precursor Missions
Phase I Final Report

John Brophy (PI), James Polk, Leon Alkalai, Bill Nesmith,
Jonathan Grandidier, *Jet Propulsion Laboratory, California Institute of Technology*
Philip Lubin; *University of California, Santa Barbara*

Executive Summary

Our breakthrough propulsion architecture is an innovative way to take advantage of kilometer-scale, multi-hundred megawatt, space-based, phased-array lasers to enable rapid transportation throughout the solar system. In this architecture, the laser would beam power over distances of up to 40 AU increasing the available power density relative to solar insolation by two orders of magnitude. The receiving vehicle would have a photovoltaic array with cells tuned to the laser frequency that outputs a voltage of 6 kV to directly-drive a lithium-fueled gridded ion thruster system at an ultra-high specific impulse of 40,000 s. Such a system could enable final spacecraft speeds of greater than 40 AU/year, potentially enabling missions to the solar gravity lens focus at 550 AU in less than 15 years. This is the propulsion architecture of the 22nd century.

Detailed analyses performed in Phase I study continue to support the original concept and indicate that spacecraft speeds of > 40 AU/year should be achievable. System architecting efforts led to different design solutions that have the potential to reduce the physical size of the laser aperture, reduce the size of the receiving photovoltaic array on the spacecraft, lower the maximum power level of the lithium ion propulsion system, reduce the required specific impulse from 58,000 s to 40,000 s and still maintain the 40 AU/year final spacecraft speed. Significant feasibility issues still need to be addressed including: The use of a beacon to phase-lock the array with round-trip light times of hours; photovoltaic arrays with output voltages of at least 6 kV; and mitigating the risk of lithium contamination on the vehicle. Follow-on investigations should include the following activities: (1) Demonstrating that photovoltaic (PV) coupons can be operated at more than 6 kV in the plasma environment created by the lithium-ion propulsion system. (2) Demonstrating PV cell efficiency of 50% or greater for monochromatic inputs. (3) Modeling the characteristic of the lithium plasma plume created by the ion propulsion system. (4) Demonstrating operation of a small aperture (0.3 m to 1 m dia.), low power (a few hundred watts) phased array with long a coherence length and beacon feedback that is scalable to large apertures. (5) Investigation of beacon phase locking for long round-trip light time delays. (6) Investigating laser location impacts on cross-track thrust.

I. Introduction

Practical interstellar precursor missions—missions to distances of 550 AU or greater—require the development of a space transportation architecture capable of providing spacecraft speeds at least an order of magnitude greater than the fastest spacecraft ever flown. The Voyager 1 spacecraft used gravity assists from Jupiter and Saturn to reach its current speed of 3.6 AU/year, making it humanity's fastest spacecraft. Our breakthrough propulsion architecture is targeting spacecraft speeds of greater than 40 AU/year. At this speed, a spacecraft would reach the solar gravity lens focus location (~550 AU from the sun [1]) in less than 15 years.

The key to the development of any system for rapid space transportation is the ability to process a lot of power with little dry mass, combined with the ability to provide a very high total spacecraft velocity change (ΔV) without a lot of propellant. These two requirements translate into the need for a very low specific mass (kg/kW) and a very high specific impulse. Our transportation architecture is targeting a spacecraft specific mass of 0.25 kg/kW, which is approximately a factor of a thousand less than the 300-kg/kW specific mass of the Dawn spacecraft. The solar-powered ion propulsion system on the Dawn spacecraft provided a total ΔV to the spacecraft of just over 11 km/s, far higher than any propulsion system in the history of human spaceflight. The ultra-low specific mass in our breakthrough architecture is enabled by removing the power source and most of the power conversion hardware from the spacecraft and replacing them with a lightweight, photovoltaic (PV) array and direct-drive configuration. The PV array outputs electric power at the voltage needed to drive a lithium-fueled, gridded ion thruster system at a specific impulse of 40,000 s. For comparison, the Dawn ion propulsion system produces a maximum specific impulse of 3,000 s. With this combination of ultra-low specific mass (0.25 kg/kW) and ultra-high specific impulse (40,000 s) missions with total ΔV's of 100 to 200 km/s become possible.

Our architecture enables 100-km/s ΔV missions this by combining the following three key innovations:
1. A phased-array laser with a kilometer-scale aperture operating steady-state in the 100-MW-class power range. This laser array is used to beam power across the solar system.
2. A 70% efficient photovoltaic array tuned to the laser frequency is used to collect the laser power and output electrical power at the voltage needed to directly drive the lithium-fueled ion propulsion systems (~6 kV).
3. A multi-megawatt, direct-drive, lithium-fueled ion propulsion system with a specific impulse of 40,000 s.

This architecture provides a breakthrough way to take advantage of very high-power lasers, of the type described by Lubin [2], to provide fast transportation though out the solar system and beyond for conventionally-sized spacecraft. One of our key innovations is the recognition that such an array increases the power density of photons available to a spacecraft illuminated by the laser beam by two orders of magnitude relative to solar insolation at all the solar system distances beyond five AU (Fig. 1) and that this can then be used to great effect by driving a highly-advanced ion propulsion system.

The highly-advanced ion propulsion system uses a high-voltage PV array tuned to the laser frequency to convert the laser power to electric power at an efficiency of 70% (efficiencies of > 60% are suggested by [3] for a 1064 nm wavelength laser). The PV array is configured to produce an output voltage of 6 kV, which is about sixty times greater than the current state of the art (~160V). The 6-kV output voltage is used directly to provide the net accelerating voltage for

the ion propulsion system eliminating the heavy, inefficient, power processing hardware, and the associated thermal radiators, typically needed to drive ion propulsion systems.

The lithium-fueled, gridded ion propulsion system provides a specific impulse of 40,000 s, roughly 20 times the current state of the art. Lithium stores as a solid, is easily ionized, and is very difficult to doubly ionize. Modeling suggests that this should allow the thruster to be operated with nearly 100% ionization of the propellant, effectively eliminating neutral gas leakage from the thruster and the production of charge-exchange ions that are responsible for thruster erosion and current collection on the photovoltaic arrays. This key benefit enables very long thruster life and facilitates the development of the 6-kV photovoltaic array.
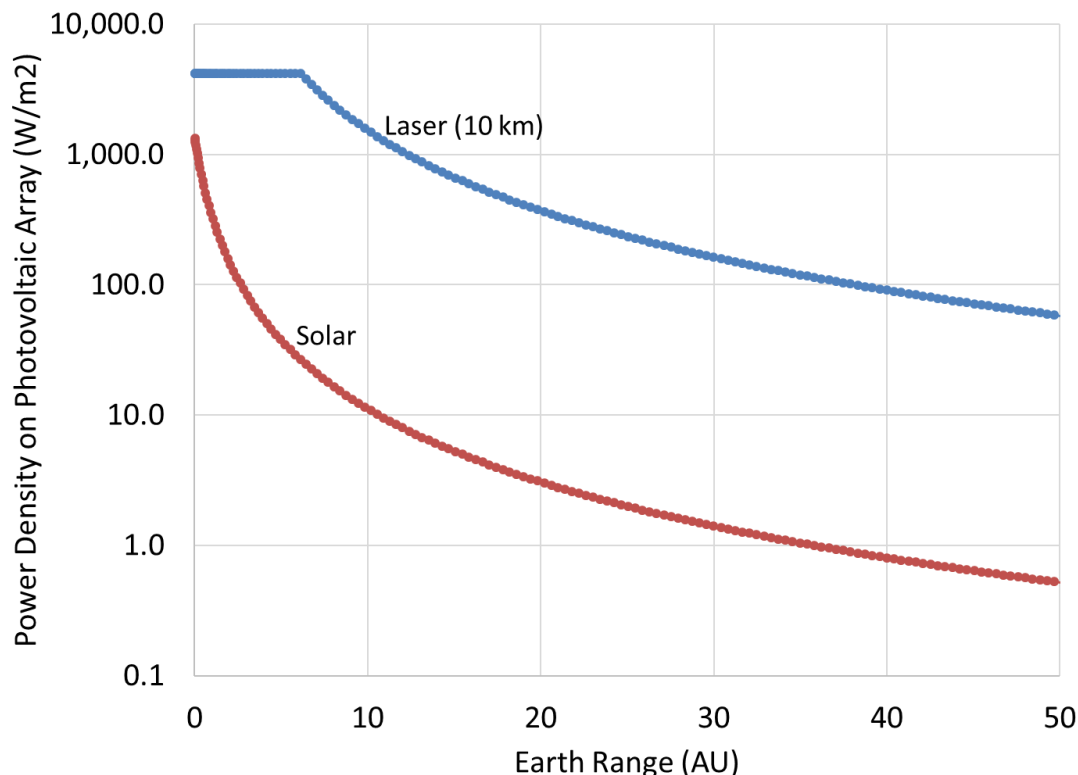
Fig. 1. A 10-km laser provides two orders of greater photon flux than the sun at ranges greater than ~5 AU.

This report summarizes the results of the Phase I effort that focused on addressing the key feasibility issues including:

1. How to minimize the laser aperture size.
2. How to minimize the size of the PV array.
3. Determination of the best combination of power level and specific impulse for the ion propulsion system.
4. Estimating the specific mass of the ion propulsion system and spacecraft.
5. Estimating the areal density of the PV array.
6. Evaluating the practicality of pointing the laser to hit the spacecraft over tens of AU distances.
7. Evaluating how to navigate the spacecraft.

II.   Phased-array Laser Technology

a. State-of-the-art

The current state of laser phased arrays is primarily focused on high power DoD directed energy systems for tactical use and for low power wafer and chip level laser communications. These have very different issues and use very different technologies. Neither of them is focused on the extremely large aperture we require. Neither of these are high TRL for space applications, though the DoD is high TRL for ground applications.

Most phased arrays are operated in a MOPA (Master Oscillator Power Amplifier) design where one master oscillator (MO-seed laser) is split via fiber optics for DoD applications and on wafer in chip/wafer scale laser comm and then then each channel of the spilt common laser seed is phase shifted for beam formation and fine steering and then amplified using one laser amplifier (PA) per split channel (Fig 2).
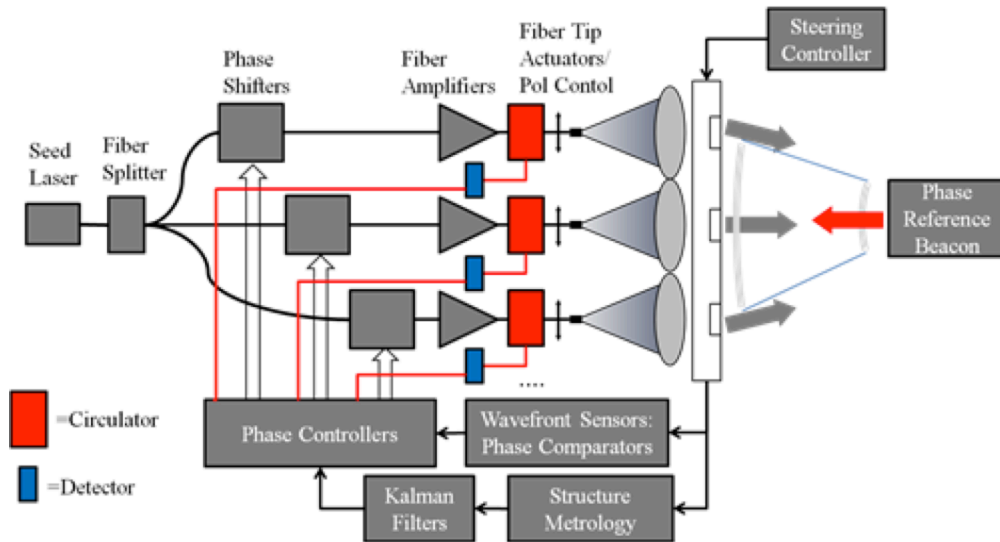
Fig. 2. Phased Array MOPA design with reference beacon for phase locking [4]. This is the basic design we propose for this program. The amplifier can be fiber based or other such as semiconductor. The phase reference beacon is on the spacecraft.

In the DoD applications, the phased array is primarily used for beam combining prior to beam injection into the final optical system, though there is some work on small aperture level phased arrays. The latter is closer to our needs but the current SOA uses apertures that are less than 1 m in diameter. The DoD focus does not need nor want large apertures for operational reasons and hence there is little overlap in this area. Typical DoD aperture needs for operational systems are sub meter. For reference, the ABL (Air Borne Laser) system, which flew on a converted 747 aircraft and used a chemical laser, had a 1.5 m aperture and was not a phased array. Current DoD applications are designed for small aperture and high aperture flux (typically > 100 kW$_{optical}$/m$^2 \sim 100$ sol) with optical power levels of about 100-300 kW$_{optical}$. Target flux is much higher as the beam is focused on the target. This is a rapidly evolving field with large

R&D and deployment budgets measured in the 10^8-10^9/year. Phased arrays are primarily being used with injection into the main (conventional) final optical element via an ODE (optical diffractive element). One of the primary differences is the required coherence length of the laser power amplifiers. In both the DoD and laser comm applications the aperture is very small (compared to our needs) so the coherence length of the amplifiers required is also very small (of order the phasing aperture) or typically cm coherence length. For our needs with 1-10 km apertures we use the same MOPA design but require laser amplifiers with much longer coherence length (typically >10 km). Another fundamental difference between DoD applications and ours is the aperture flux we need is much less. We have a trade space between aperture size and total optical power. For example, in our original system design we needed a power level of order 100 MW$_{optical}$ spread over a 10-km aperture. This gives an aperture flux of about 1 W$_{optical}$/m^2 ~ 10^{-3} sol. The combination of vastly lower aperture flux (compared to DoD applications) and the vastly larger coherence length changes the amplifier and system design significantly. This offers both opportunities (semiconductors and novel fiber amplifiers for example) as well as challenges. Some of the challenges are economic in nature. There is both a technical trade space with power and aperture size as well as an economic trade space. There is a trade between optical costs (larger apertures cost more for optics) but require lower total power (hence less cost for laser amplifiers) while smaller apertures require lower cost for the optics but require larger power and hence more cost for laser amplifiers. Since the laser amplifiers are photonics devices and are an exponentially growing technology (like electronics) this will tend to favor higher laser power (as the costs are dropping with time). This is being actively pursued as part of the NIAC Phase II DEIS (Starlight) program.

b. Development opportunities and challenges

The development of a space-based large aperture phased array represents a significant technological challenge from many points. Whether orbital- or lunar-based, such a system has many challenges from photonics and optics to structural metrology and stability. There is an important and critical difference between a narrow bandwidth phased array and a large optical telescope design. A phased array is essentially an ideal adaptive optical system with every sub element being electronically phase controlled. The phase required is modulo 2π and does NOT require absolute phase matching. We only require phase control to within the coherence length of the amplifiers. This is vastly different than a large aperture telescope where absolute path matching is required. This means the phase control is not a mechanical (stiffness) requirement as it would be on telescope but a servo loop control bandwidth issue. This dramatically simplifies the design of the optical structure and dramatically reduces the stiffness requirement.

Fortunately, we can also leverage the large amount of efforts in related fields that feed into this. These include the DoD small aperture efforts as well as the exponential growth in photonics, especially integrated wafer-scale photonics. The amount of yearly funding going into photonics alone is comparable to the entire NASA budget and will continue to grow as it is driven by diverse societal needs. Our low power per sub element needs are ideally suited to benefit from the growth in integrated photonics and is currently the focus of Starlight program. The exponential growth in performance and price reduction both have doubling times that are currently about 1.5 years (based on the last 25 years) which is similar to the "Moore's Law" in the semiconductor electronics industry. Integrated photonics is also a semiconductor based industry and is just beginning to blossom and will drive prices down dramatically as it has for

solid state lighting. For reference, the current cost of high power (kilowatt) fiber amplifiers (Yb based at 1.06 microns) is about \$50-\$100/$W_{optical}$ in modest quantities. However, this is for power levels that are much higher than we need and for coherence lengths much smaller than we need. As a comparison, the cost of solid state GaN based LED's is already about \$0.1/$W_{optical}$ in large quantities and dropping. One of the goals being explored as a part of the Starlight program is to focus on low cost fiber and semiconductor based amplifiers with a cost goal of approaching the current solid state lighting costs. Even at 100x the current solid state lighting costs (or \$10/$W_{optical}$), the laser amplifier costs for a 100 $MW_{optical}$ laser would not be the dominant cost. While building a kilometer scale space based array is a formidable challenge, it is much different than building a kilometer-scale telescope and has an "exponentially growing photonics engine" behind it.

# III. Propulsion System Architecture Scaling

As described in the introduction, one of the keys to achieving a very high spacecraft speed is to minimize the spacecraft's specific mass. During Phase I, we divided the spacecraft into the following major components and then assessed the specific mass of each component: the photovoltaic array, the electric propulsion subsystem (which includes the power distribution system), and the spacecraft structure. These are the most massive components of the vehicle. The rest of the spacecraft subsystems were assumed to be allocated to a mass consistent with a conventionally-sized spacecraft such as New Horizons [5].

a. Photovoltaic Array Areal Density

Areal Density Scaling with Array Size.

The areal density estimate of 200 g/m^2 assumed in the original proposal was based largely on estimates from Reed and Willenberg [6]. They estimated that an ultra-lightweight array with an areal density of 100 g/m^2 was feasible, which we doubled to add some conservatism. Their estimate was based on a system that used ultra-lightweight carbon-fiber reinforced polymer booms with thin-film solar cells (CFRP TFSC). More recently, Arya, Lee, and Pellegrino [7] have also estimated that large (60 m x 60 m) deployable space structures for solar power satellites with an areal density of 100 g/m^2 are possible.

In the Phase I study, we based the PV receiver array on an inflatable structure from L'Gard combined with thin-film solar cells. The mass breakdown for a 175-m diameter array is given in Table 1. Subsequent analysis (given in Section III.d of this report) indicate that 110-m diameter array could be sufficient. The estimated areal density as a function of array diameter is given in Fig. 3. These estimates support the assumption that an areal density of approximately 200 g/m^2 is feasible. An illustration of the resulting spacecraft configuration is given in Section III.c.
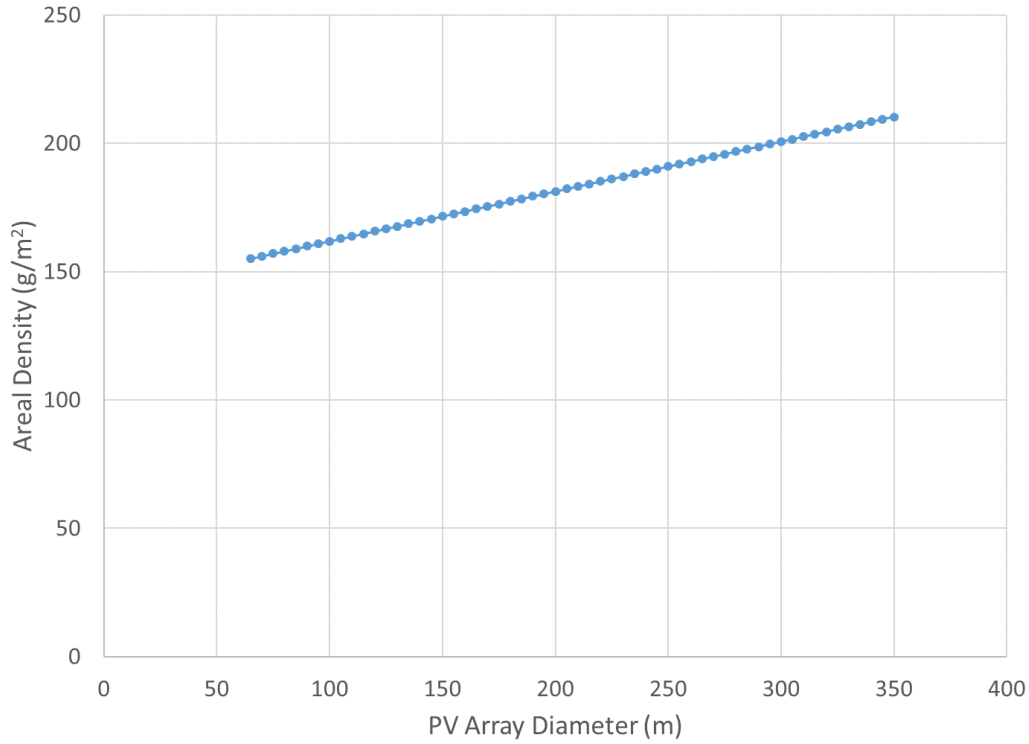
Fig. 3. Areal density for the PV Receiver Array based on the inflatable structure design from L'Gard and thin film solar cells.

Cell Efficiency. State-Of-Practice (SOP) solar cell efficiency is around 30% and the bare cell weight is around 850 g/m^2. Table 2 shows characteristics of SOP solar cells for three major space solar cell vendors. Initial calculations show that using thin film flexible Copper Indium Gallium Diselenide (CIGS) could reduce the solar cell mass density to 67.2 g/m^2, which is essential for achieving a total PV array areal density close to our target value of 200 g/m^2. However, the highest efficiency measured to date with small-area single-junction efficiency for CIGS with a solar input is now around 22% [8]. Additionally, CIGS has demonstrated radiation hardness in space environment [9]. These characteristics potentially makes CIGS an appealing candidate for a light-weight flexible solar array, but significantly higher efficiencies are needed for our application. The key feasibility question is can efficiencies of 50% or greater be obtained with thin-film cells tuned to the laser frequency. This issue will be addressed in Phase II.

6-kV Output Voltage Feasibility. The output voltage of the photovoltaic receiver array must be at least 6 kV in order to directly drive the lithium ion propulsion system to produce a specific impulse of 40,000 s. State-of-the art solar arrays are designed for nominal operating voltages of up to 160 V. Flight tests of small arrays have demonstrated operation at 300 V. Ground tests in a plasm environment have demonstrated successful operation at voltages as high as 1 kV. These tests demonstrated that high output voltage operation can be achieved through proper cell separation distances/packing factors and grouting, suggesting that there is a reasonable expectation that operation at 6 kV is feasible. We will investigate experimentally this in Phase II.

Table 1. Circular PV Array (175m Diameter) with 6 Radial Spokes

Element	Value	Unit
Diameter of PV Array	175	m
Thickness of Kapton Substrate	5	μm
Mass Density of Kapton Substrate	1384	kg/m^3
Areal Mass Density of PV Array (CIGS)	67.2	g/m^2
Fraction of Membrane Area Populated by PVs	85	%
Number of Radial Structural Support Spokes	6	
Base Diameter of Support Spoke	10	m
Tip Diameter of Support Spoke	1	M
Wall Thickness of Support Spoke	127	μm

Element	Value (kg)
Substrate	183
Photovoltaics	1374
Structural Support Spokes	1870
Inflation Tank (Qty:4: 0.3m x 1m cylinder)	693
Inflatant Mass	123
Total System Mass	**4243**
Total Areal Density	**180 g/m^2**

Table 2: Solar cell characteristics for State-Of-Practice solar cells from the two main US space solar cell venders Spectrolab and SolAero, and the European vendor Azur Space.

Solar cell	Spectrolab		SolAero	Azur Space	
	UTJ	XTJ	ZTJ	3G28	3G30
Composition	GaInP2 GaAs Ge	GaInP2 GaAs Ge	InGaP InGaAs Ge	InGaP GaAs Ge	InGaP GaAs Ge
BOL Efficiency (%)	28.3	29.5	29.5	28	30
Voc (V)	2.66	2.633	2.726	2.667	2.7
Jsc (mA/cm²)	17.05	17.76	17.4	16.77	17.24
Vmp (V)	2.35	2.348	2.41	2.371	2.411
Jmp (mA/cm²)	16.3	17.02	16.5	16.14	16.71

| Weight (g/m²)	840	840	840	860	860

b. Electric Propulsion System Scaling

The electric propulsion subsystem consists of the thrusters, the power processing units (PPUs), the lithium feed system, and the harnessing connecting the components and the photovoltaic array. We developed point designs for ion beam power levels ranging from 10 to 30 MW and beam voltages of 6000 to 12000 V (corresponding to specific impulses of 42000 to 59000 s) and estimated the masses of the individual components in order to determine the total system mass and specific mass over this trade space. The process involved first defining the number, size, and discharge power of the engines in a given system point design, then applying mass models for the components. The assumptions in the mass models and the resulting specific masses are described below.

The engines were sized based on the total power, beam voltage, and reasonable assumptions for the engine design. The total beam current was calculated from the total beam power level and voltage. The total beam area was then calculated assuming an average beam current density of 8.3 mA/cm2, which was chosen based on an ion optics design using the CEX2D code [10] with an electric field of 2500 V/mm between the grids. This electric field is similar to state-of-the-art thrusters. This current density is about 50% of the maximum current density that can be extracted from the grids, and preliminary erosion estimates indicate this should provide the required lifetime. For the lower subsystem power levels, we assumed the power was processed in ten engines, which resulted in ion beam diameters on the order of 1 to 2 m. For some of the higher power levels the number of active thrusters was increased to as high as 20 so that the beam diameter did not exceed 2 m. This is a size that can reasonably be fabricated and maintain the required grid gap. One spare thruster was included for single fault tolerance. Discharge power was calculated assuming a beam ion production cost of 200 W/A. This is a conservative value based on a model of a lithium discharge chamber operating at high propellant utilization efficiency [11].
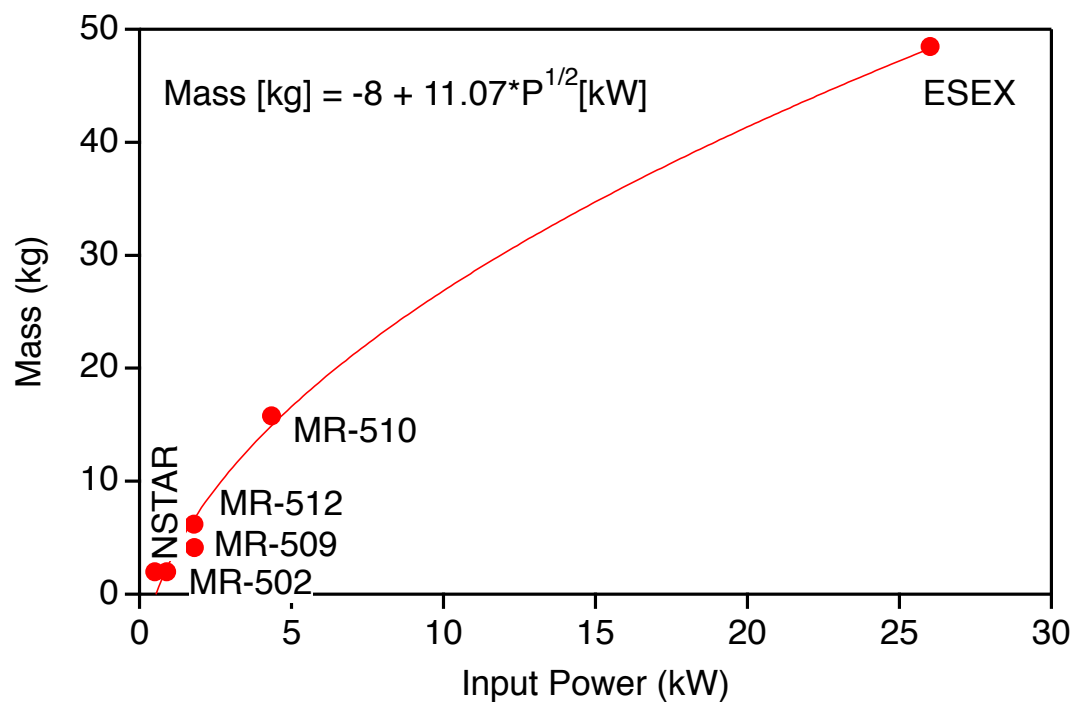
The engine mass was assumed to scale with beam area and the XIPS, NSTAR, NEXT, and NEXIS ion thrusters [12-15] were used to determine the constant of proportionality. These engines have power levels ranging from 2.5 to 20 kW and beam areas up to 0.25 m^2. As Fig. 4 shows, the masses of the NSTAR, NEXT, and NEXIS thrusters are well represented by a line with a slope of 146 kg/m^2. The 25-cm XIPS engine falls above the line, but uses an iron discharge chamber design that is inherently heavier than the design approach used in the other engines. We anticipate that the high power lithium engines will work with discharge chamber designs similar to the other thrusters.

The beam power is assumed to be supplied directly by the high voltage array, so the only component required in the PPU for the high voltage is an isolation switch. The power conditioning mass will be dominated by the mass of the discharge power converter. The point designs developed for the propulsion system mass scaling require discharge powers of 25 to 50 kW and discharge currents of 1250 to 2500 A for a discharge voltage of 20V (which is based on the lithium discharge chamber model). High power processing units tend to scale with the square root of the discharge power. Figure 5 displays the mass of the NSTAR thruster discharge power supply [13] (designed for 16 A and 30 V), four high current commercial power supplies built for arcjet thrusters [16], and a 26 kW power supply built for the ESEX high power

ammonia arcjet demonstration experiment [17] (130 V and 200 A). As the curve fit indicates, the masses of these power supplies do tend to scale with the square root of power.

Mass [kg] = 146 * A_{beam} [m^2]

NEXIS

25-cm XIPS

NEXT

NSTAR
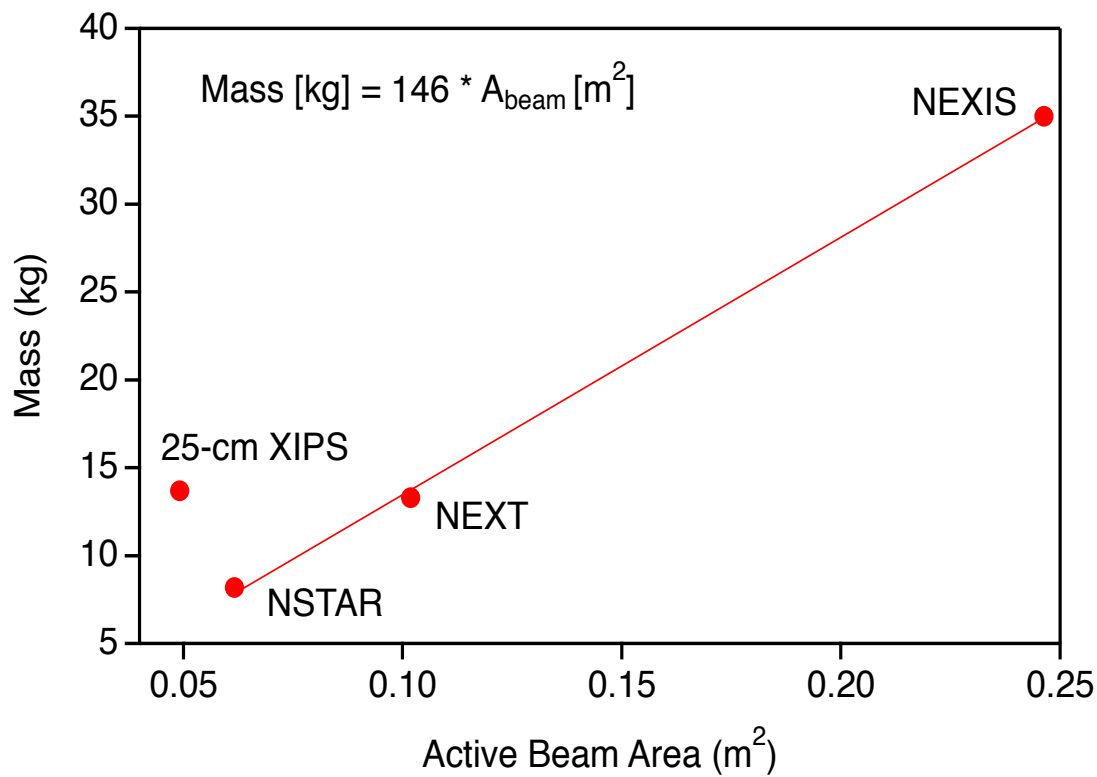
Fig. 4. Ion engine mass scaling relationship used in the propulsion system mass model.

Mass [kg] = -8 + 11.07*$P^{1/2}$[kW]

ESEX

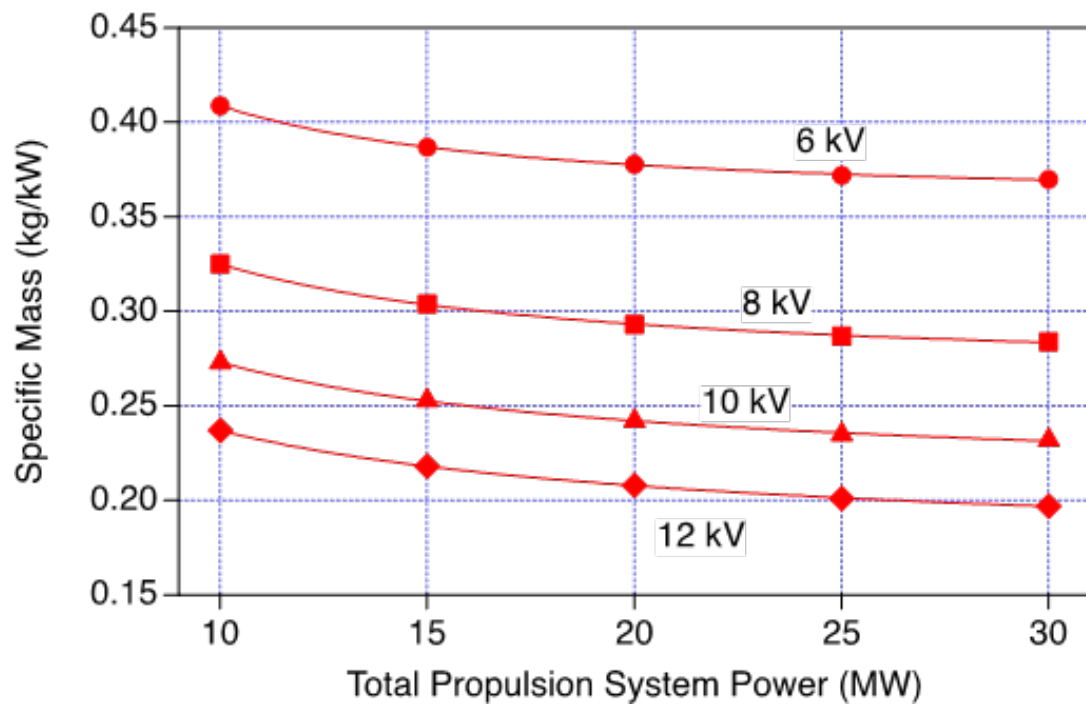MR-510

NSTAR

MR-512

MR-509

MR-502

The lithium feed system mass is based on a conceptual design originally developed for a high power lithium electromagnetic thruster [18]. This design uses high temperature valves, filters, pressure transducers, electromagnetic flow sensors and pumps, and heaters and thermal blankets for thermal management. The masses listed in Table 3 are based on similar existing components (valves and filters, for example) or laboratory model versions of less mature components (such as the electromagnetic pumps and flow meters).

The harness mass for a given thruster consists of the high voltage cable required to carry the beam current, the low voltage input for the discharge power converter (assumed to be supplied by a 100 V segment of the array), and the high current, low voltage PPU output cable. The cables connecting the PV array to the PPU were assumed to be 10 m long and the cables from the PPU to the engine 3 m long. We also assumed that the cable masses would be dominated by the copper conductors and that the insulation mass would be negligible. The conductors were sized so that the voltage drops were only on the order of a few volts and the dissipated power was low enough that it could be radiated away from the cables at moderate temperatures. This resulted in cable masses per thruster on the order of 40 kg.

The masses of the individual point designs were used to determine the total electric propulsion system mass and the specific mass for the range of system powers and beam voltages. As shown in Fig. 6, the specific mass decreases with beam voltage because the beam current for a given power level is lower, resulting in smaller engines and discharge power supplies. The specific mass drops slightly with system power because of the nonlinear scaling of some components with power. Details for 10 MW and 30 MW systems are given in Table 4 and 5. These results were used with the other subsystem models in the system trade studies.

Table 3. Mass equipment list for the conceptual feed system design.

Component	Component Mass (kg)	Quantity in Subsystem	Mass per Subsystem	Quantity in System	System Mass
Fixed Feed System			18.8	1	18.8
Manual Fill/Drain Valve	0.4	1	0.4		
Y Getter	1	1	1		
Filter	5	1	5		
Parallel Redundant Pressure Regulator					
Latch Valves	0.5	2	1		
EM Pumps/Flow Sensor	0.1	2	0.2		
Pressure Transducers	0.4	2	0.8		
Misc. Tubing	6.4	1	6.4		
Thermal Blankets			0		
Heaters			0		
Mounting Plate	4	1	4		
Feed System Per Engine			5.6	3	16.8
Flex Line	1	1	1		
Latch Valve	0.5	1	0.5		
EM Pump/Flow Sensor	0.1	1	0.1		
Misc. Tubing		1	0		
Thermal Blankets		1	0		
Heaters		1	0		
Mounting Plate	4	1	4		

Fig. 6. Specific mass as a function of total propulsion system power and beam voltage.
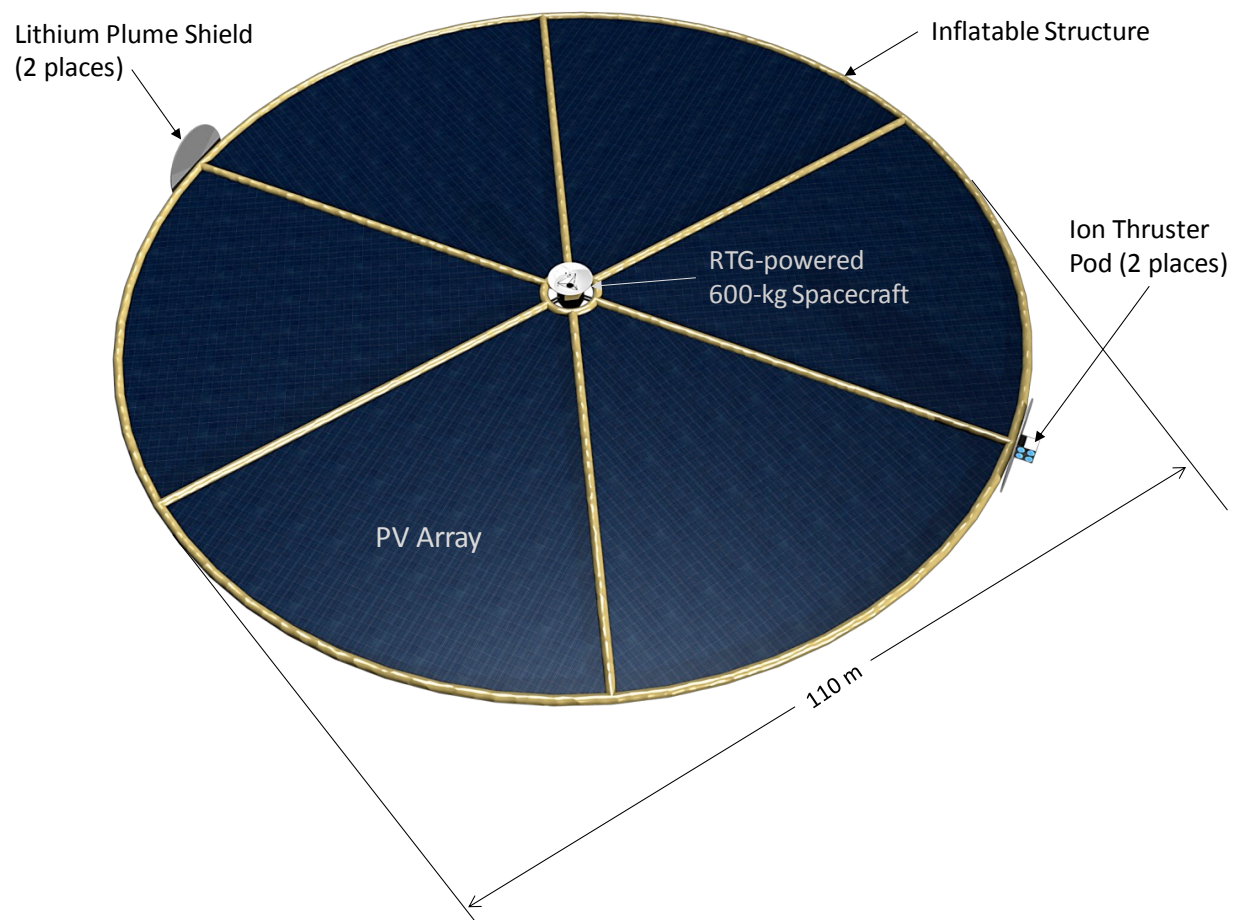
Table 4. Specific mass details for 10 MW EP systems

Total Power, Voltage, and Propellant Mass				
Beam Voltage (V) =	6000	8000	10000	12000
Total Beam Power (MW) =	10	10	10	10
Specific Impulse (s) =	41,000	47,500	53,000	58,000
Total Propellant Mass (kg) =	9000	9000	9000	9000
Thruster Power, Current, Voltage, and Size				
Discharge Loss (W/A) =	200	200	200	200
Discharge Voltage (V) =	20	20	20	20
Discharge Current/Beam Amp (A/A) =	10	10	10	10
Total Beam Current (A) =	1667	1250	1000	833
Total Discharge Current (A) =	16667	12500	10000	8333
Total Discharge Power (kW) =	333	250	200	167
Total Thruster Power (MW) =	10.33	10.25	10.20	10.17
Number of Thrusters =	10	10	10	10
Power per Thruster (MW) =	1.03	1.03	1.02	1.02
Average Beam Current Density (A/cm2) =	0.0083	0.0083	0.0083	0.0083
Beam Current per Thruster (A) =	167	125	100	83
Discharge Current/Thruster (A) =	1667	1250	1000	833
Active Beam Area per Thruster (m2) =	2.01	1.51	1.20	1.00
Grid Diameter (m) =	1.60	1.38	1.24	1.13
Thruster Mass				
Mass (kg) =	293	220	176	147
Specific Mass (kg/kW) =	0.284	0.215	0.172	0.144
Discharge Supply Mass				
Power per Thruster (kW) =	33.33	25	20	16.67
Mass per String (kg) =	55.91	47.35	41.51	37.19
Specific Mass based on total power (kg/kW) =	0.054	0.046	0.041	0.037
Discharge Current Harness (PPU to thruster, per thruster)				
Harness Length (m) =	3	3	3	3
Copper Resistivity (ohm-m) =	1.68E-08	1.68E-08	1.68E-08	1.68E-08
Copper Density (kg/m3) =	8940	8940	8940	8940
Discharge Current (A) =	1667	1250	1000	833
Conductor Diameter (cm) =	2	2	2	2
Anode + CC Resistance (ohm) =	0.0003	0.0003	0.0003	0.0003
Total Voltage Drop (V) =	0.53	0.40	0.32	0.27
Total Power Loss (W) =	890	501	320	223
Total Mass (kg) =	16.85	16.85	16.85	16.85
Beam Current Harness (PV to PPU, PPU to thruster, per thruster)				
Total Harness Length (m)	13	13	13	13
PV to PPU Harness Length (m) =	10	10	10	10
PPU to Thruster Harness Length (m) =	3	3	3	3
Copper Resistivity (ohm-m) =	1.68E-08	1.68E-08	1.68E-08	1.68E-08
Copper Density (kg/m3) =	8940	8940	8940	8940
Beam Current (A) =	167	125	100	83
Conductor Diameter (cm) =	0.5	0.5	0.5	0.5
Anode + NC Resistance (ohm) =	0.0222	0.0222	0.0222	0.0222
Total Voltage Drop (V) =	3.70	2.78	2.22	1.85
Total Power Loss (W) =	617	347	222	154
Total Mass (kg) =	4.56	4.56	4.56	4.56
Discharge Current Harness (PV to PPU per thruster)				
Harness Length (m) =	10	10	10	10
Copper Resistivity (ohm-m) =	1.68E-08	1.68E-08	1.68E-08	1.68E-08
Copper Density (kg/m3) =	8940	8940	8940	8940
Discharge Current (A) =	1667	1250	1000	833
Discharge Voltage (V) =	20	20	20	20
Bus Voltage (V) =	100	100	100	100
Bus Current (A) =	333	250	200	167
Conductor Diameter (cm) =	1	1	1	1
Anode + CC Resistance (ohm) =	0.0043	0.0043	0.0043	0.0043
Total Voltage Drop (V) =	1.42	1.07	0.85	0.71
Total Power Loss (W) =	475	267	171	119
Total Mass (kg) =	14.04	14.04	14.04	14.04
Total Thruster/PPU/PMAD				
Total Mass (kg)	4230	3330	2782	2412
Specific Mass (kg/kW)	0.409	0.325	0.273	0.237
Misc.				
Tankage (5% of Prop Mass, kg) =	450	450	450	450
Structure (4% of wet mass, kg) =				
All other S/C bus subsystems (allocation)	500	500	500	500
Instruments	100	100	100	100

Table 5. Specific mass details for 30 MW EP systems

Total Power, Voltage, and Propellant Mass				
Beam Voltage (V) =	6000	8000	10000	12000
Total Beam Power (MW) =	30	30	30	30
Specific Impulse (s) =	41,000	47,500	53,000	58,000
Total Propellant Mass (kg) =	9000	9000	9000	9000
Thruster Power, Current, Voltage, and Size				
Discharge Loss (W/A) =	200	200	200	200
Discharge Voltage (V) =	20	20	20	20
Discharge Current/Beam Amp (A/A) =	10	10	10	10
Total Beam Current (A) =	5000	3750	3000	2500
Total Discharge Current (A) =	50000	37500	30000	25000
Total Discharge Power (kW) =	1000	750	600	500
Total Thruster Power (MW) =	31.00	30.75	30.60	30.50
Number of Thrusters =	20	15	12	10
Power per Thruster (MW) =	1.55	2.05	2.55	3.05
Average Beam Current Density (A/cm2) =	0.0083	0.0083	0.0083	0.0083
Beam Current per Thruster (A) =	250	250	250	250
Discharge Current/Thruster (A) =	2500	2500	2500	2500
Active Beam Area per Thruster (m2) =	3.01	3.01	3.01	3.01
Grid Diameter (m) =	1.96	1.96	1.96	1.96
Thruster Mass				
Mass (kg) =	440	440	440	440
Specific Mass (kg/kW) =	0.284	0.215	0.172	0.144
Discharge Supply Mass				
Power per Thruster (kW) =	50.00	50	50	50.00
Mass per String (kg) =	70.28	70.28	70.28	70.28
Specific Mass based on total power (kg/kW) =	0.045	0.034	0.028	0.023
Discharge Current Harness (PPU to thruster, per thruster)				
Harness Length (m) =	3	3	3	3
Copper Resistivity (ohm-m) =	1.68E-08	1.68E-08	1.68E-08	1.68E-08
Copper Density (kg/m3) =	8940	8940	8940	8940
Discharge Current (A) =	2500	2500	2500	2500
Conductor Diameter (cm) =	2	2	2	2
Anode + CC Resistance (ohm) =	0.0003	0.0003	0.0003	0.0003
Total Voltage Drop (V) =	0.80	0.80	0.80	0.80
Total Power Loss (W) =	2003	2003	2003	2003
Total Mass (kg) =	16.85	16.85	16.85	16.85
Beam Current Harness (PV to PPU, PPU to thruster, per thruster)				
Total Harness Length (m)	13	13	13	13
PV to PPU Harness Length (m) =	10	10	10	10
PPU to Thruster Harness Length (m) =	3	3	3	3
Copper Resistivity (ohm-m) =	1.68E-08	1.68E-08	1.68E-08	1.68E-08
Copper Density (kg/m3) =	8940	8940	8940	8940
Beam Current (A) =	250	250	250	250
Conductor Diameter (cm) =	0.5	0.5	0.5	0.5
Anode + NC Resistance (ohm) =	0.0222	0.0222	0.0222	0.0222
Total Voltage Drop (V) =	5.55	5.55	5.55	5.55
Total Power Loss (W) =	1389	1389	1389	1389
Total Mass (kg) =	4.56	4.56	4.56	4.56
Discharge Current Harness (PV to PPU per thruster)				
Harness Length (m) =	10	10	10	10
Copper Resistivity (ohm-m) =	1.68E-08	1.68E-08	1.68E-08	1.68E-08
Copper Density (kg/m3) =	8940	8940	8940	8940
Discharge Current (A) =	2500	2500	2500	2500
Discharge Voltage (V) =	20	20	20	20
Bus Voltage (V) =	100	100	100	100
Bus Current (A) =	500	500	500	500
Conductor Diameter (cm) =	1	1	1	1
Anode + CC Resistance (ohm) =	0.0043	0.0043	0.0043	0.0043
Total Voltage Drop (V) =	2.14	2.14	2.14	2.14
Total Power Loss (W) =	1068	1068	1068	1068
Total Mass (kg) =	14.04	14.04	14.04	14.04
Total Thruster/PPU/PMAD				
Total Mass (kg)	11455	8728	7091	6000
Specific Mass (kg/kW)	0.370	0.284	0.232	0.197
Misc.				
Tankage (5% of Prop Mass, kg) =	450	450	450	450
Structure (4% of wet mass, kg) =				
All other S/C bus subsystems (allocation)	500	500	500	500
Instruments	100	100	100	100

14

c. Laser-powered Electrically-propelled Vehicle (LEV) Configuration

As a result of the Phase 1 investigation, the configuration for the Laser-powered Electrically-propelled Vehicle (LEV) shown in Fig. 7 was developed. This vehicle is dominated by the large, 110-m-diameter, photovoltaic (PV) receiver array that collects the laser power to operate the lithium-ion propulsion system. The PV array consists of an inflatable structure with a PV blanket based on thin-film solar cells. The PV array outputs the voltage of 6 kV to 10 kV necessary to directly accelerate lithium ions to the required specific impulse of 40,000 s to 50,000 s.

Lithium Plume Shield
(2 places)

Inflatable Structure

Ion Thruster
Pod (2 places)

RTG-powered
600-kg Spacecraft

PV Array

110 m

Fig. 7. Configuration of the Laser-powered, Electrically-propelled Vehicle (LEV) based on the Phase I investigation. The vehicle includes a 110-m-diameter photovoltaic array for receiving the beamed laser power, a 10-MW lithium-fueled ion propulsion system that produces a specific impulse of 40,000 s, and a 600-kg RTG-power spacecraft located at the center of the PV array.
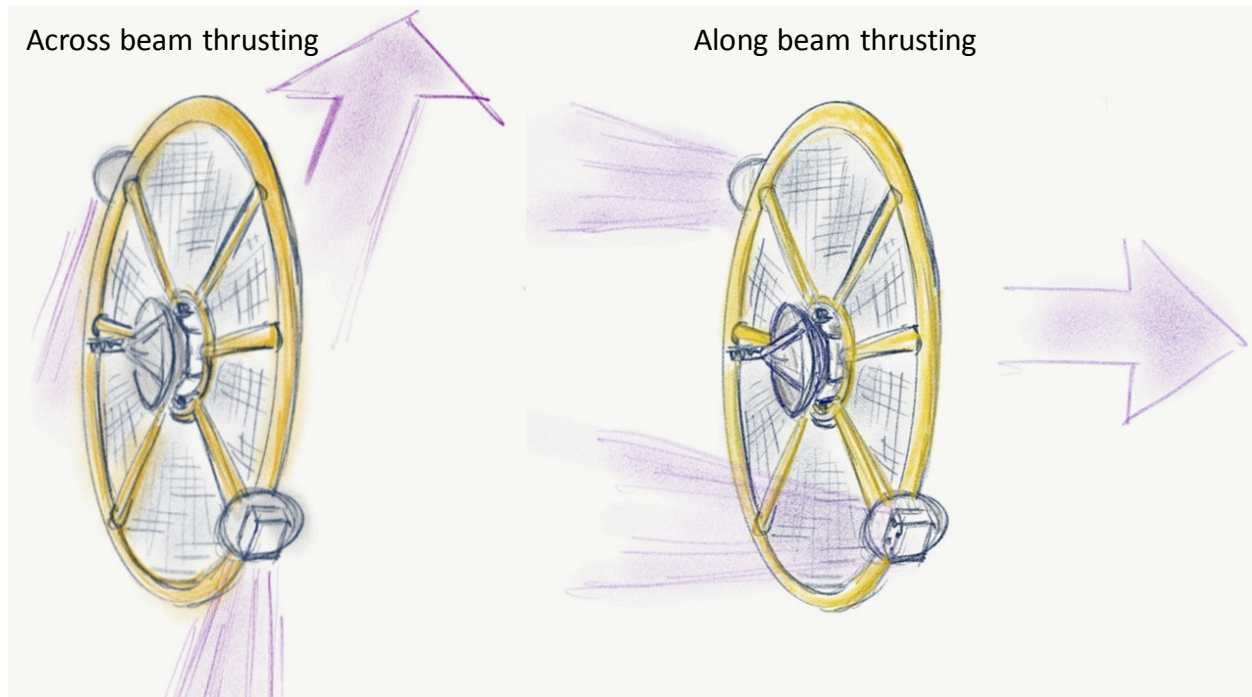
Fig. 8. Illustration of the LEV's ability to thrust across the laser beam (left) or along it (right), assuming the beam is coming in from the left side of the page normal to the surface of the LEV's PV array.

The lithium ion thrusters are located in two pods on the periphery of the PV array at opposite ends of two inflatable struts across the diameter of the array. The lithium propellant is stored at the center of the PV array where the RTG-power spacecraft is located. Each ion thruster pod is attached to a two-axis gimbal that enables the system to thrust in a direction along the laser beam or across it, as indicated in Fig. 7. Lightweight plume shields are located between the ion thruster pods and the PV array to minimize the deposition of lithium on the array. The lithium-ion thrusters are equipped with slotted ion optics with the long dimension of the slots pointing toward the center of the of the PV array. This configuration of the ion optics results in very small ion beam divergence, of order 1 degree, in the direction along the slots. Consequently, this design will minimize the interaction of the high-power lithium ion beams with the rest of the LEV.

d. Architecture Systems Engineering

The originally-proposed breakthrough architecture assumed the existence of a 100-MW phased-array laser with a 10-km aperture that beamed power over tens of AU to the LEV equipped with a 175-m diameter photovoltaic receiver array. The laser wavelength was assumed to 1064 nm and the cell efficiency of the PV array was assumed to be 70%. The spacecraft's electric propulsion system was assumed to be capable of processing a maximum of 70 MW at a

specific impulse of 58,000 s. In this section, we describe the results of a systems architecting activity designed to investigate the tradeoffs between laser aperture size, laser power level, PV receiver array size, specific impulse, and maximum power processing capability of the electric propulsion system. In addition, this section also summarizes the results of a study to investigate the sensitivity of the spacecraft performance, as indicated by its final speed, to the PV areal density, the PV cell efficiency, and the electric propulsion subsystem specific mass.

Laser Scaling. In the original proposal, the phased-array laser was assumed to have an aperture of 10 km. The reason for this large aperture is illustrated in Fig. 9 where the ratio of power density provided by the laser array to solar insolation is given as a function of distance from the Earth. These curves indicate, for example, that at 10 AU, a 1-km laser aperture with a wavelength of 1064 nm provides little better than twice the solar insolation. A 5-km laser aperture would provide nearly 60 times the solar insolation at 10 AU, but a 10-km aperture provides over 200 times the solar insolation. However, a 10-km laser with a power level of 100 MW as originally assumed would have a power density of just 1 W/m^2. Such a low power density suggests that a better trade between laser aperture size and power level is possible.
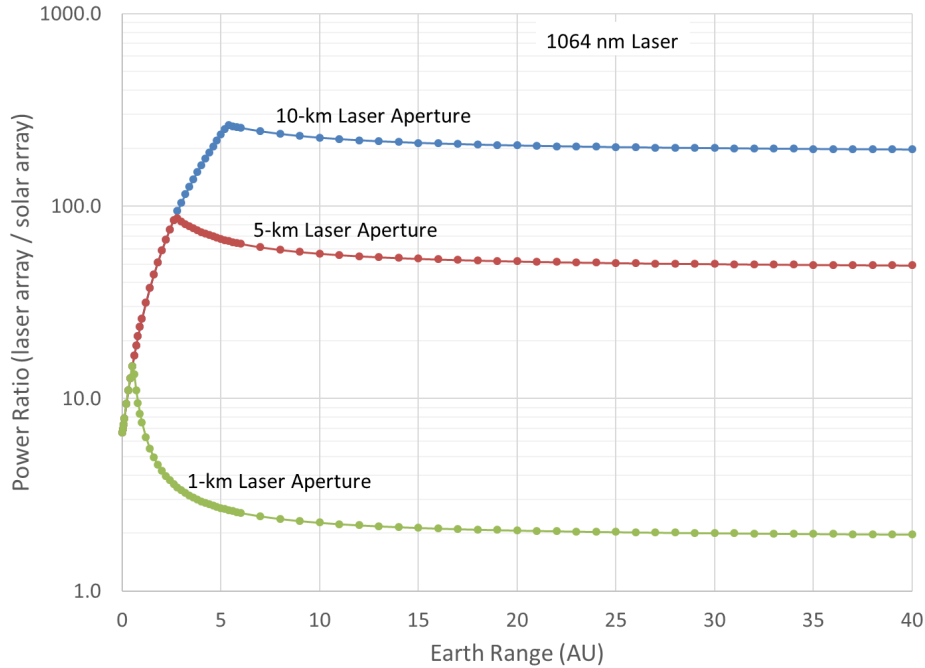

Fig. 9. Very large phased-array laser apertures are necessary to provide a power density that is more than 100x the solar insolation at large ranges.

Laser power delivered to a 175-m diameter PV array is given in Fig. 10 as a function of range for different combinations of laser aperture size and power level. It is clear from this figure that smaller-aperture, higher-power lasers can provide the same performance in terms of delivered power as the very large aperture laser assumed in the original proposal. This is simply a representation of Eq. (1) for diffraction-limited optics, where d is the diameter of the laser spot size, R is the range, λ is the laser wavelength, and D is the diameter of laser aperture.

$$d = 2R\lambda/D. \tag{1}$$

The power incident on the PV array is fraction of the laser spot area intercepted by the PV array times the laser power. The combinations of laser power levels, aperture sizes, and wavelengths in Fig. 10 were selected to all provide the same power to the PV array for ranges larger than about 5 AU. The corresponding laser spot sizes and the fractions of the laser power intercepted by the PV array are given in Fig. 11.
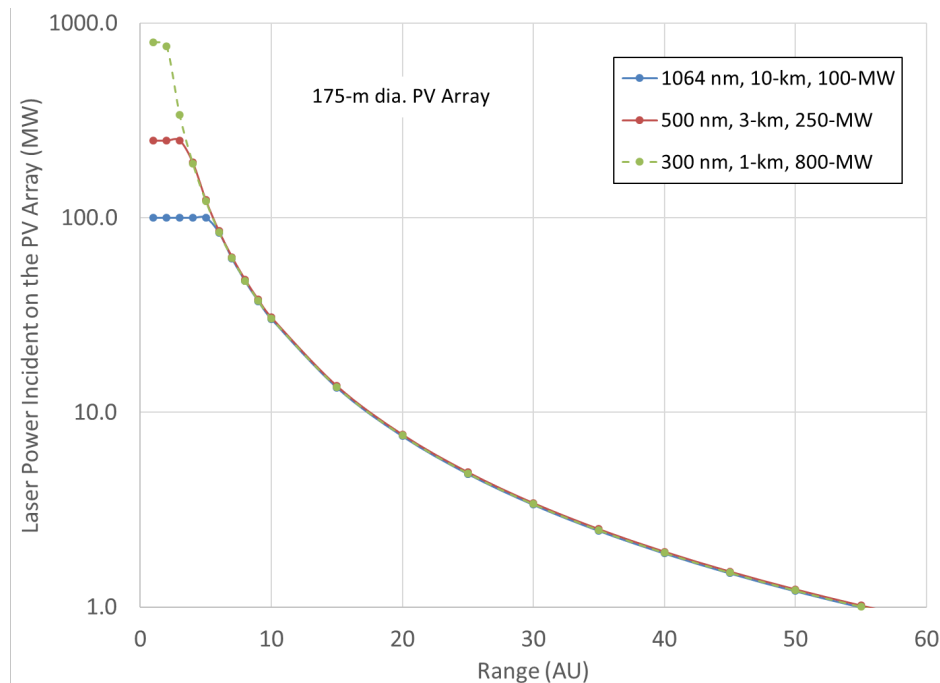
Fig. 10. Smaller, higher power, higher frequency lasers can provide the same power to the spacecraft as a function of distance as larger, lower power, lower frequency ones.
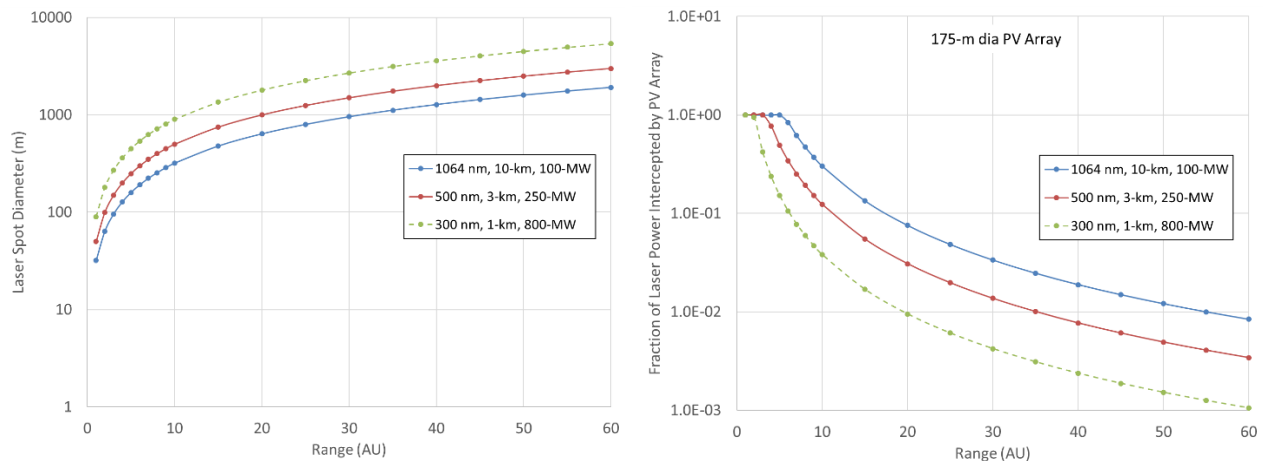
Fig. 11. Larger aperture lasers provide a smaller spot size as a function of distance (left) resulting in a higher fraction of the laser being intercepted by the PV array (right), but this difference can be compensated by operating the smaller laser at a higher power level to provide the same total power to the array as indicated in Fig. 10.

18

It is clear from Fig. 11 that at large ranges the PV array intercepts only a small fraction of the laser power. For example, at 20 AU, a 175-m diameter PV array intercepts only 1% of the 300-nm, 1-km, 800-MW laser power. But 1% of 800 MW is still 8 MW. If the PV array converts this to electrical power at 70% efficiency, then this approach would provide 5.6 MW of electrical power to the spacecraft at 20 AU. For comparison, a conventional solar array (with 30% efficient cells at 1 AU) would have to have a diameter of about 1.3 km to provide 5.6 MW of electrical power at 20 AU. Assuming a conventional flexible blanket array could be constructed of this size and assuming this array had a specific power of 500 W/kg at 1 AU (~5x better than the current state of the art for flexible blanket arrays), then this 1.3 km diameter array would have a mass of 4,600,000 kg. Our 175-m diameter PV array, with an areal density of 200 g/m^2 would have a mass of just 4800 kg, roughly a thousand times lower mass.

In the sections that follow, the final speed of the Laser-powered, Electrically-propelled Vehicle (LEV) is calculated based on the following assumptions:
1. The laser spot size is the diffraction-limited value.
2. The spacecraft is continuously illuminated by the laser.
3. Gravity losses are neglected.
4. The spacecraft thrusts directly away from the laser in the direction of the laser beam propagation.
5. Thrusting is terminated after the spacecraft reaches 40 AU from the laser.
6. Thrusting duty cycle is assumed to be 100%.
7. Thrust losses associated with cross-track thrusting to maintain the spacecraft inside the laser beam are neglected.

With these assumptions, the final spacecraft speed for a system based on a 1064-nm phased-array laser is given as a function of laser power in Fig. 12 for three different laser apertures, 2-km, 5-km, and 10-km. The LEV is assumed to have a 110-m-diameter PV receiver array with an areal density of 200 g/m^2 and a cell efficiency of 70%. The electric propulsion system on the LEV is assumed to have a maximum power processing capability of 10 MW, with a specific impulse of 40,000 s and an efficiency of 97%. These values are different from those used in the original proposal and are the result of the scaling and sensitivity analyses provided below.

The objective of the system architecture design is to provide a final spacecraft speed of at least 40 AU/year. The green curve (corresponding to the 10-km laser aperture with a wavelength of 1064 nm) in Fig. 12 at a laser power of 100 MW provides a final spacecraft speed of 40 AU/year. This is approximately the point design assumed in the original proposal. The red curve in Fig. 12 indicates that a spacecraft speed of 40 AU/year could also be achieved with a 5-km, 1064-nm laser by increasing the power to 400 MW. The 2-km, 1064-nm laser cannot enable spacecraft speeds of 40 AU/year even at 1000 MW.

Corresponding results are given in Fig. 13 assuming a 300-nm laser. Such lasers don't currently exist, but there is a reasonable expectation that they could be developed in the future. The blue curve in Fig. 13 indicates that a 2-km laser operating at 300 nm and 200 MW could enable spacecraft speeds of 40 AU/year. The green curve in Fig. 13 saturates at higher power levels because of the assumption that the electric propulsion system cannot process more than 10 MW of power. The spacecraft speed plateaus because the laser is providing more power than can be used by the spacecraft. In subsequent analyses we will assume the use of a 2-km, 300-nm laser with an output power of 300 MW. This provides a final spacecraft speed of 43 AU/year as indicated in Fig. 13.

Photovoltaic Array Scaling. The photovoltaic receiver array on the LEV is one of the key technologies enabling the breakthrough propulsion architecture. This array has three key requirements. First, it must be very lightweight, with areal densities of order 200 g/m^2. Second, the PV cells must have a high efficiency (> 50%) for the conversion of laser power to electrical power. Third, the array must output the voltage required by the lithium-ion thrusters to produce the desired specific impulse. Voltages of order 6 kV to 10 kV are expected to be required.
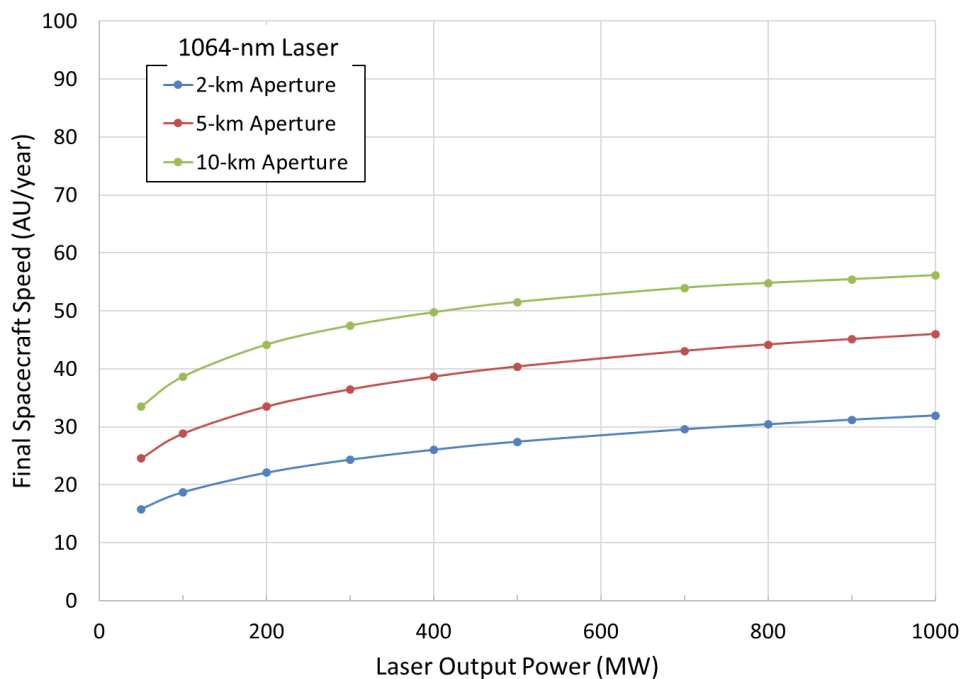
Fig. 12. For a 1064-nm laser and a specific impulse of 40,000-s EP system, aperture diameters of 5-km or more are necessary to enable final spacecraft speeds of at least 40 AU/year.
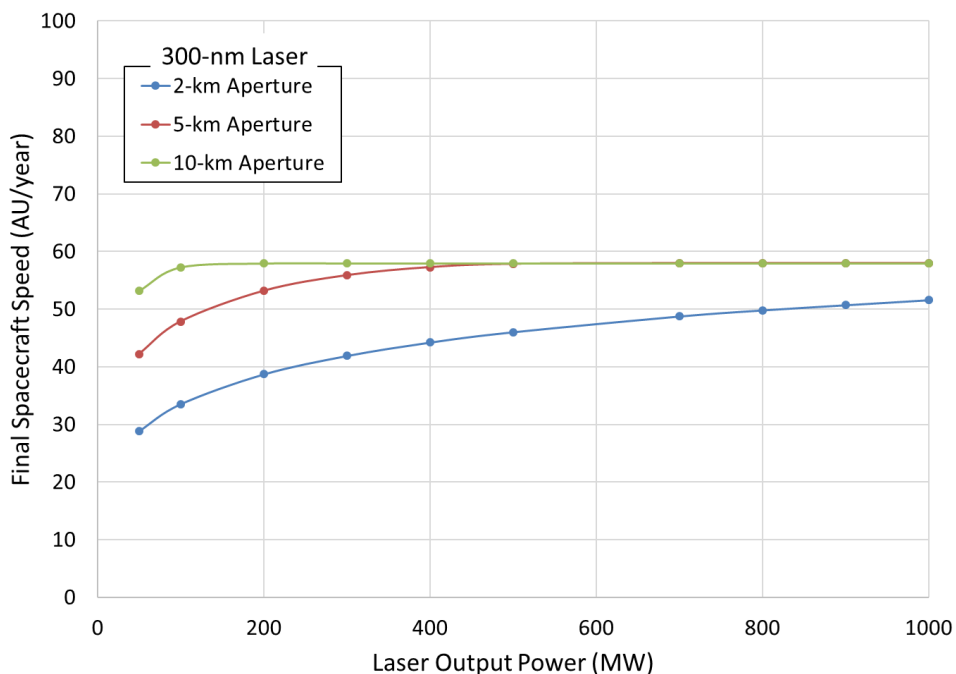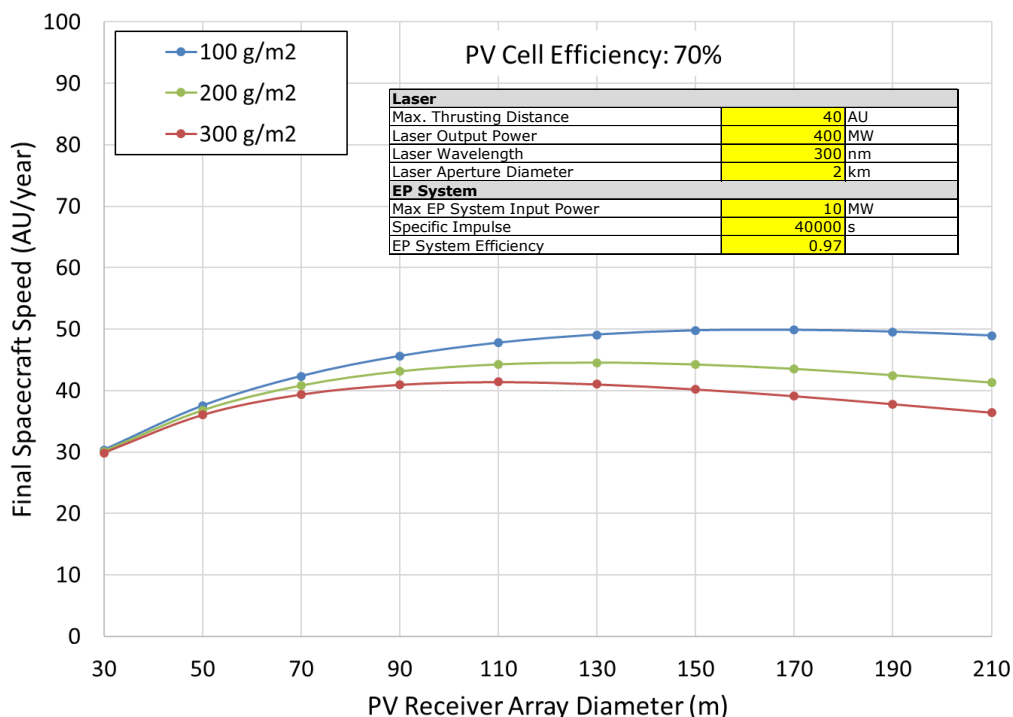
Fig. 13. For a 300-nm laser and a 40,000-s EP system, an aperture diameter of 2-km can enable final spacecraft speeds of at least 40 AU/year.

This section of the report looks at the sensitivity of the final spacecraft speed to the receiver array mass, size, and cell efficiency. The mass of the receiver array is expressed in terms of the areal density (mass per unit area). The final spacecraft speed is given as a function of the diameter of the spacecraft PV receiver array in Fig. 14 for three different areal densities assuming cell efficiency of 70%. As expected, lower areal densities (lighter PV arrays) result in higher final spacecraft speeds. At an array diameter of 130 m, the difference in speeds is about 10 AU/year in going from an areal density of 300 g/m^2 to 100 g/m^2. For an areal density of 200 g /m^2, the optimum array size is approximately 110 m diameter, but the final spacecraft speed is insensitive to the PV array diameter over the range of roughly 90 m to 150 m.

The effect of PV cell efficiency on the final spacecraft speed is given in Fig. 15 for a PV array areal density of 200 g/m^2. The optimum PV array diameter is insensitive to the cell efficiency. To achieve final spacecraft speeds of greater than 40 AU/year, PV cell efficiencies of at least 50% are required. However, the system performance is not very sensitive to efficiencies between 50% and 70%.

Electric Propulsion Subsystem Scaling. Three main parameters determine the performance of the electric propulsion system: specific impulse, specific mass, and maximum input power. The first key issue is to determine approximately the right range for the specific impulse. It is relatively easy to see from the rocket equation that the exhaust velocity needs to be within a factor of two or so of the characteristic velocity for the mission. Since we are targeting missions with characteristic velocities in the range 100 to 200 km/s, we would expect to need an exhaust velocity in the range 50 km/s to 400 km/s. These exhaust velocities correspond to specific impulses in the range 5,000 to 40,000 s.

Laser		
Max. Thrusting Distance	40	AU
Laser Output Power	400	MW
Laser Wavelength	300	nm
Laser Aperture Diameter	2	km
EP System		
Max EP System Input Power	10	MW
Specific Impulse	40000	s
EP System Efficiency	0.97	

Fig. 14. The final spacecraft speed is a weak function of the PV array diameter with optimum diameter between 90 m and 150 m depending on the areal density. Final spacecraft speeds of greater than 40 AU/year are possible even with array areal densities as high as 300 g/m^2.
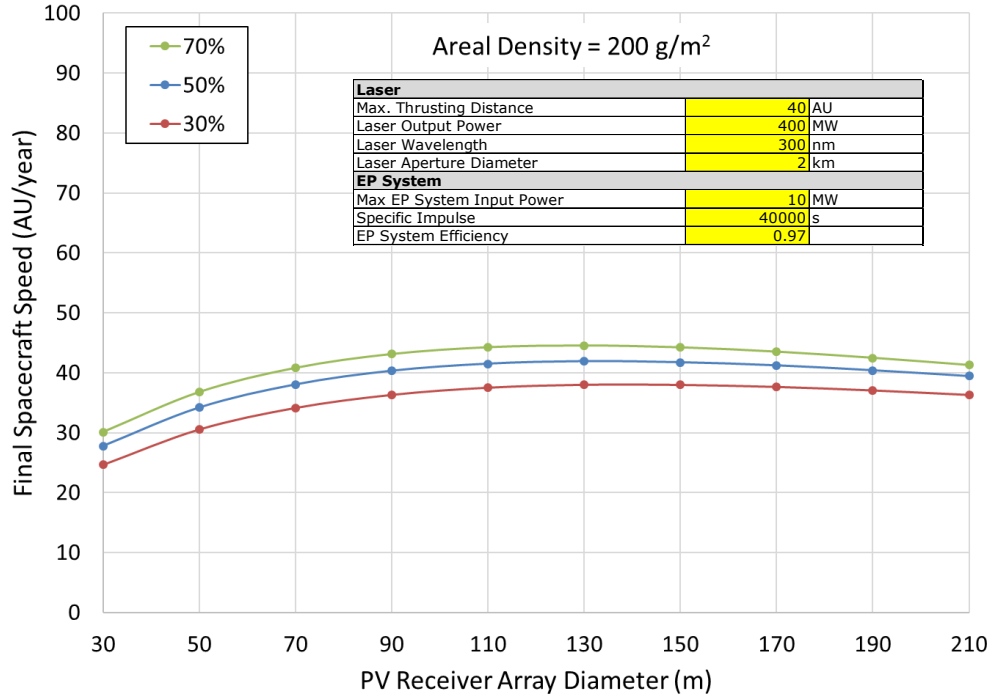
Fig. 15. The PV cell efficiency in the range 30% to 70% has virtually no impact on the optimum PV array diameter. Cell efficiencies of roughly 50% or greater are necessary to achieve final spacecraft speeds of greater than 40 AU/year.

The final spacecraft speed is given as a function of maximum input power to the electric propulsion system in Fig. 16 over the range of specific impulses from 5,000 s to 50,000 s. These data indicate that the final spacecraft speed is largely independent of the maximum EP system power, with a slight advantage for lower power levels. Significantly, specific impulses of around 50,000 s are required to enable spacecraft speeds of greater than 40 AU/year. For the data in Fig. 16, the specific mass of the EP system has been scaled as a function of specific impulse using the process given in Section III.b.
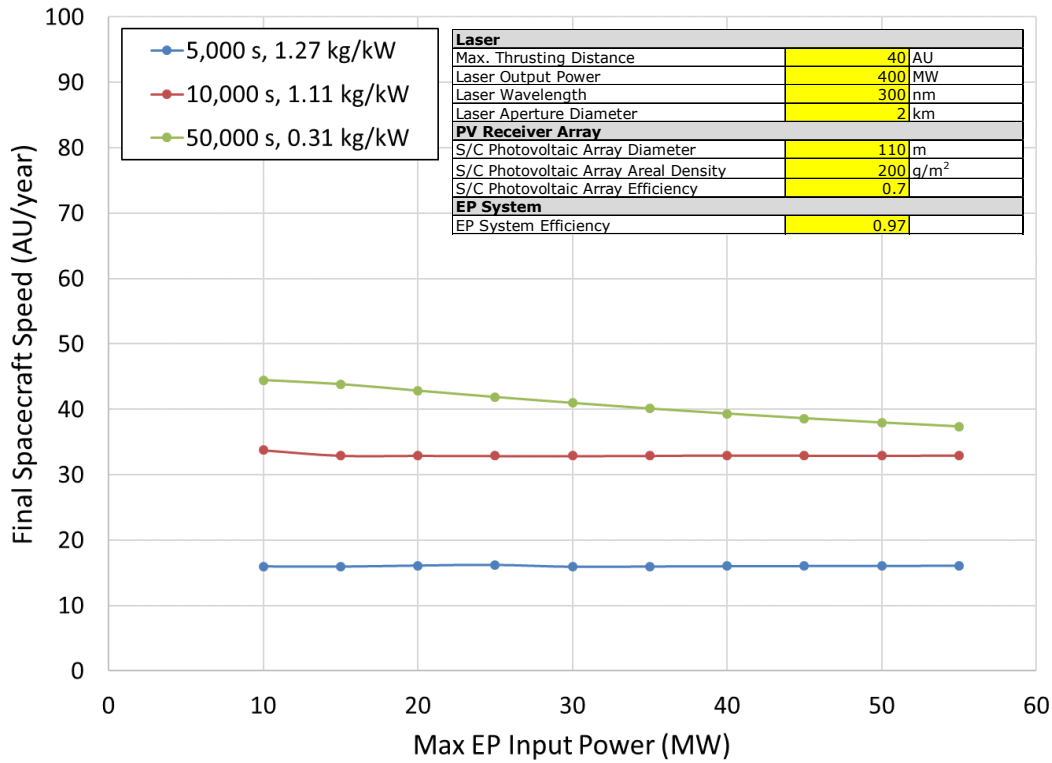
The thrust of a laser-sail is given by,

$$T_{sail} = \frac{P_0(1 + \varepsilon_r)}{c}$$

where P_0 is the laser power, ε_r is the reflection (=1 for complete reflection), and c is the speed of light. But, an electric propulsion vehicle that converts the laser power into electric power can

convert a large fraction of the total power in the laser beam to thrust. The thrust for an electric propulsion system is,

$$T_{EP} = \frac{2\eta P_0 \varepsilon_a}{I_{sp} g}$$

where η is the EP system efficiency (assumed to be 0.97), ε_a is the conversion efficiency of the photovoltaic array, I_{sp} is the specific impulse, and g is gravitational acceleration at the Earth's surface. Combining these two equations gives the ratio of thrusts for a laser-driven electric propulsion system and a laser-drive sail as,

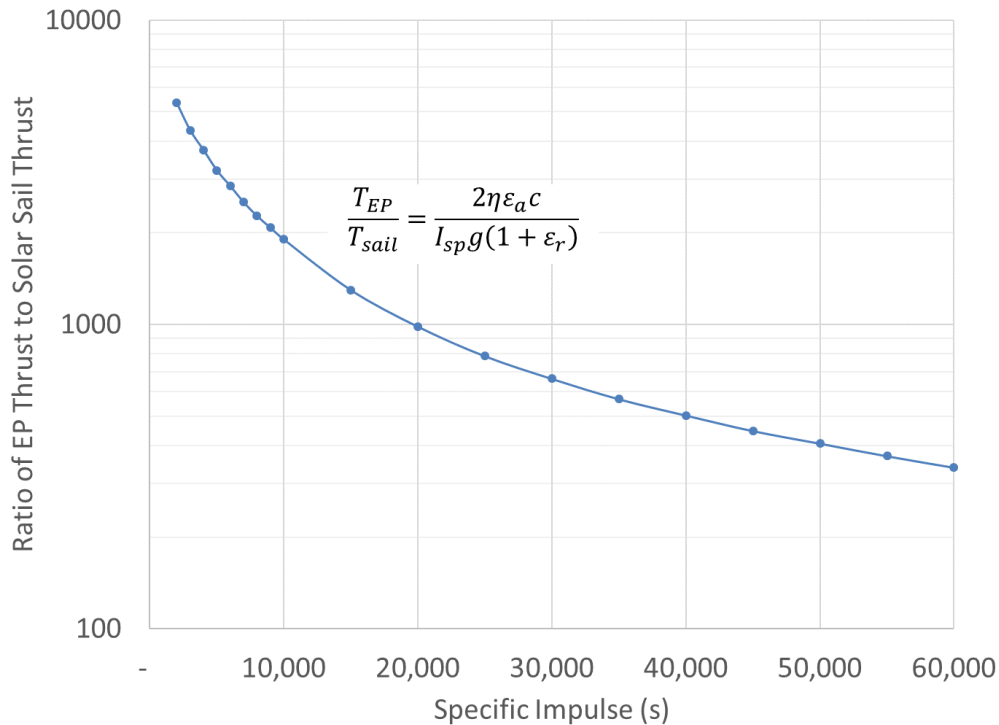| Laser		
Max. Thrusting Distance	40	AU
Laser Output Power	400	MW
Laser Wavelength	300	nm
Laser Aperture Diameter	2	km
PV Receiver Array		
S/C Photovoltaic Array Diameter	110	m
S/C Photovoltaic Array Areal Density	200	g/m²
S/C Photovoltaic Array Efficiency	0.7	
EP System		
EP System Efficiency	0.97	

Fig. 16. Specific impulses of around 50,000 s are necessary to achieve spacecraft speeds of greater than 40 AU/year.

$$\frac{T_{EP}}{T_{sail}} = \frac{2\eta \varepsilon_a}{(1 + \varepsilon_r)} \left(\frac{c}{I_{sp} g} \right)$$
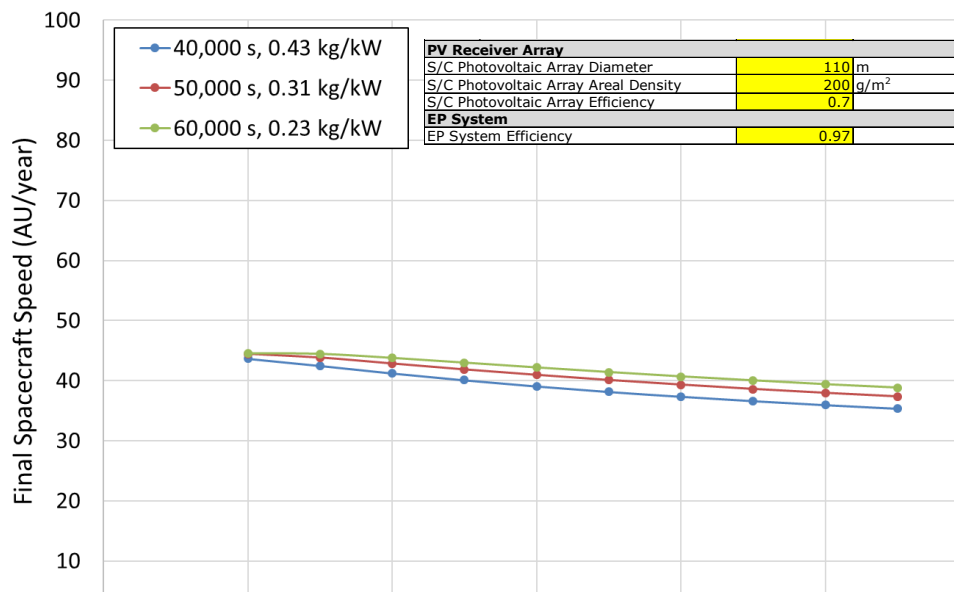
Significantly, this ratio does not depend on the laser power, but is primarily a function of the ratio of the EP system specific impulse to the speed of light. This equation is plotted in Fig. 17 assuming $\varepsilon_a = 0.7$, $\varepsilon_r = 1$, and η varies with specific impulse from 0.5 at 2000 s to 0.97 at 60,000 s. This figure indicates that at a specific impulse of 40,000 s the electric propulsion system produces that thrust level that is approximately 500 times greater than that of a laser sail. This means that EP-based vehicles could be 500 times as massive as a laser-sail vehicle for the same acceleration.

Focusing in on the range of specific impulses from 40,000 s to 60,000 s, the final spacecraft speed is given as a function of maximum input power in Fig. 18. The final spacecraft speed is insensitive to specific impulse over this range, with higher values giving slightly higher final speeds. The highest speeds still occur at the lowest EP system input powers.

In the previous analyses, the system specific masses were taken from the scaling analyses presented in Section IIIa and IIIb. In Fig. 19, the effect of varying the total vehicle specific mass over two orders of magnitude from 0.25 kg/kW to 25 kg/kW is presented. It is clear from this figure that very low specific masses are required to achieve spacecraft speeds of greater than 40 AU/year. This supports the architecture in this study that is designed around minimizing the LEV specific mass.

$$\frac{T_{EP}}{T_{sail}} = \frac{2\eta\varepsilon_a c}{I_{sp}g(1+\varepsilon_r)}$$

Fig. 17. At a specific impulse of 50,000 s, an electric propulsion based vehicle produces approximately 400 times the thrust of a laser-propelled sail for the same laser power.

PV Receiver Array		
S/C Photovoltaic Array Diameter	110	m
S/C Photovoltaic Array Areal Density	200	g/m²
S/C Photovoltaic Array Efficiency	0.7	
EP System		
EP System Efficiency	0.97	

- 40,000 s, 0.43 kg/kW
- 50,000 s, 0.31 kg/kW
- 60,000 s, 0.23 kg/kW

Fig. 18. Varying the specific impulse in the range 40,000 to 60,000 s has only a small effect on the final spacecraft speed.
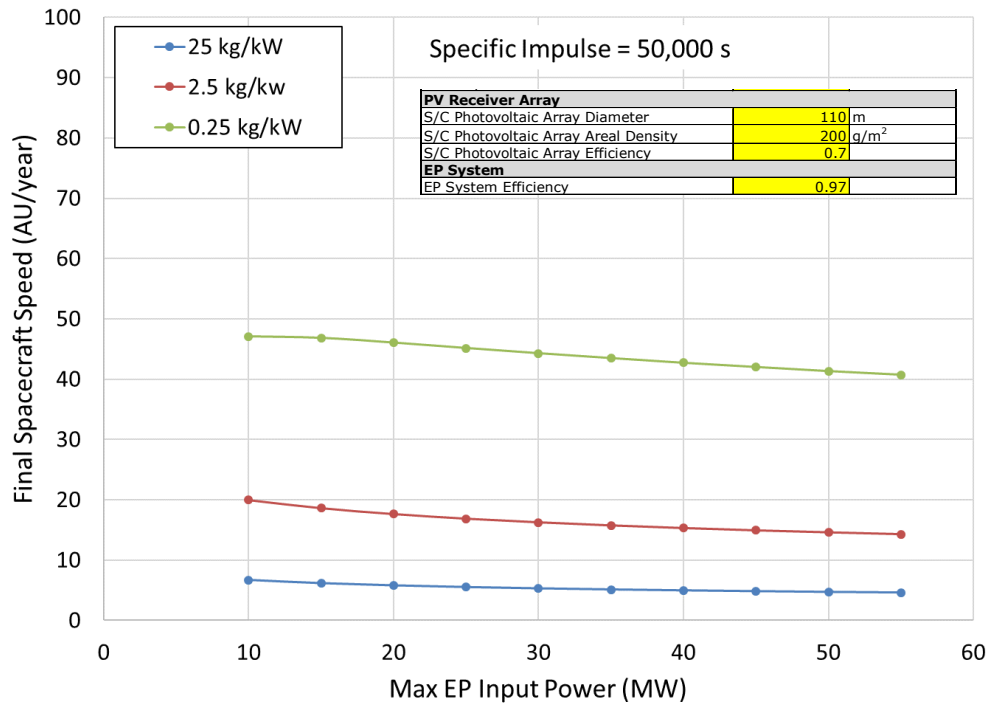
Fig. 19. Specific masses of order 0.25 kg/kW are necessary to achieve final spacecraft speeds of greater than 40 AU/year.

IV. Navigation Considerations

There are two key issues associated with the navigation of the laser-driven spacecraft and pointing of the laser. These issues are how to start-up the system at any range up to 40 AU (i.e., re-acquire the spacecraft by the laser beam), and how to keep the spacecraft in the beam during thrusting.

a. Startup

For startup, the laser beam must acquire the spacecraft. For a 110-m diameter PV array and a 2-km laser aperture with a 300 nm laser wavelength, the laser spot size is equal to the PV array

size at a distance of 2.44 AU. At this distance, the PV array subtends an angle of 0.3 nradians as viewed from the laser transmitter. The current Delta-Differential One-Way Ranging (Δ-DOR) radio navigation capability based on X-band is about 2 nradians, which is not sufficient. To get the required angular position accuracy, we assume the use of a laser beacon on the LEV combined with distributed telescopes on the edges of the 2-km laser to receive the beacon. We also require that the error between the angular measurement of the spacecraft position as determined by the distributed telescopes and the laser beam direction is small.

The startup process is to measure the spacecraft position based on detection of the laser beacon, hit the LEV with the high-power laser and then allow time for the spacecraft to travel to the center of the beam. This requires that the spacecraft be able to measure its position relative to the laser beam center.

Startup at 2.44 AU. At 2.44 AU, the diameter of the laser spot is the same as the diameter of the PV array. The one-way light time is 20 minutes. With the above assumptions, if the beam hits the spacecraft, the spacecraft is already relatively close to the center of the beam, so the time required to center the spacecraft in the beam is small.

Startup at 40 AU. At 40 AU, for a 2-km laser aperture with a 300 nm wavelength, the spot size is 1800 m. The one-way light time is 330 minutes. If the spacecraft is within the beam it will receive $(110/1800)^2$ or 0.3% of the total beam power. For a 400 MW laser this is 1.2 MW. At a specific impulse of 50,000 s, this results in a thrust of 4.75 N. For a spacecraft mass of 6,000 kg, the spacecraft could move over half the beam with (900 m) in about 18 minutes assuming all of the thrusting is in the radial (across beam) direction. This is a reasonable startup duration.

b. Thrusting

For normal thrusting three simultaneous control loops are envisioned. The first one is a short loop where the spacecraft chases the laser beam in order to stay centered within the beam. The second is a longer loop where the laser array adjusts the pointing profile with a time constant based on the round trip light time to the spacecraft. The final control loop is a much longer-term one that updates the desired thrusting profile. This final control loop would likely have a time constant of a week or a few weeks.

It is important that the spacecraft be capable of determining where it is inside the laser beam once the beam illuminates it. This will provide even more accurate information regarding the spacecraft position than that provided by the beacon. It is assumed that the LEV provides this information continuously back to the high-power laser. The spacecraft must have sufficient cross-track (cross-beam) thrust capability to stay within the laser beam. Purely cross-track thrusting is probably the most stressing case and sufficient thrust margin would need to be built in to the trajectory to prevent the spacecraft from falling out of the beam.

Missed Thrust. No missed thrust margin has been built into the performance estimates at this time. Since typical missed thrust margins are of the order 10% or so, this is not a significant impact at this conceptual stage of the concept development. After thrusting ends, however, whether planned or unplanned, it will be necessary to use the laser-array telescope measurements of the spacecraft beacon to reestablish the starting conditions.

c. Requirements

The above discussion was used to derive the following requirements for the system:
1. The high-power phased-array laser must be capable of measuring the spacecraft angular position with the same resolution as the laser beam diameter.
2. The high-power phased-array laser array must be capable of directing the power beam with an angular error that is small compared to the measurement error of the spacecraft's angular position.
3. The LEV must provide a laser beacon to the large laser array even when not illuminated by the high-power laser.
4. The LEV must be able to measure its position in the power beam.
5. The LEV must be able to communicate to the large laser array during thrusting to provide information regarding its position within the power beam.

V. Summary/Conclusions

The Phase I analyses indicate that the concept of using a very large aperture, space-based, phased-array laser to beam power across the solar system to a vehicle equipped with an ultra-high specific impulse ion propulsion system to achieve spacecraft speeds of greater than 40 AU/year continues to look feasible. A systems architecting activity and sensitivity analyses conducted during the Phase I period identified alternate configurations based on original overall system architecture that provide a better balance of technology development difficulty across all elements of the architecture. For example, by assuming the development of high-efficiency, steady-state lasers with wavelengths in the range of 300 nm in the future (instead of the 1064 nm assumed in the original proposal), the laser aperture could be reduced from 10 km to 2 km. This, however, will come at the expense of increasing the laser power from 100 MW to 400 MW. In addition, it was found that key characteristics of the Laser-powered Electrically-propelled Vehicle (LEV) could be relaxed. For example, the size of the PV receiver array on the LEV was reduced from 175 m diameter to 110 m. The PV cell efficiency requirement was reduced from 70% to 50%, the specific impulse of the lithium-fueled ion thrusters could be reduced from 58,000 s to 40,000 s, which would enable a reduction in the required output voltage from the PV receiver array from 12 kV to 6 kV. While we do not claim that these new values represent the optimum set of parameter values for this architecture, the Phase I results indicate that spacecraft speeds of greater than 40 AU/year can be achieved with combinations of parameter values that may be easier to achieve than assumed in the original proposal.

Acknowledgments

References

1. Turyshev, S.G., B.G. Anderson, "The 550 AU Mission: A Critical Discussion," MNRAS 341 (2003) 577-582, gr-qc/0205126.
2. Lubin, P., "A Roadmap to Interstellar Flight," NIAC Phase I Final Report, 2015.
3. Takeda, Y., et al, "Silicon photovoltaic cells coupled with solar-pumped fiber lasers emitting at 1064 nm," Journal of Applied Physics, 116, 014501 (2014).
4. Lubin, P. "The Roadmap to Interstellar Flight", Journal of the British Interplanetary Society – JBIS, vol. 69, pp.40-72, 20 (2016).
5. https://en.wikipedia.org/wiki/New_Horizons
6. Reed, K. and Willenberg, H. "Early commercial demonstration of space solar power using ultra-lightweight arrays," Acta Astronautica 65 (2009) 1250-1260.
7. Arya, M., Lee, N., and Pellegrino, S., "Ultralight Structure for Space Solar Power Satellites," 3rd AIAA Spacecraft Structures Conference, San Diego, CA, 4-8 January 2016.
8. Green MA, Hishikawa Y, Dunlop ED, Levi DH, Hohl-Ebinger J, Ho-Baillie AWY. Solar cell efficiency tables (version 51). Prog Photovolt Res Appl. 2018;26:3–12, https://doi.org/10.1002/pip.2978.
9. Kawakita, S., et al., "Flight Data of a Cu(In,GA)Se2 Thin-Film Solar Cell Module with a Coverglass by a Nano Satellite," Tran. JSASS Space Tech. Japan, Vol. 7, No ists26, pp. Ph_49-Ph_53, 2009.
10. Wirz, R.E., Anderson, J.R. and Katz, I., "Time-Dependent Erosion of Ion Optics," J. Propulsion and Power, Vol. 27, No. 1, January-February 2011
11. Brophy, J.R., Polk, J.E., and Goebel, D.M., "Development of a 50,000-s, Lithium-fueled, Gridded Ion Thruster," IEPC-2017-042, Presented at the 35th International Electric Propulsion Conference, Georgia Institute of Technology • Atlanta, Georgia • USA, October 8 – 12, 2017.
12. Goebel, D.M., et al., "Performance of XIPS Electric Propulsion in On-Orbit Station Keeping of the Boeing 702 Spacecraft," AIAA 2002-4348, 38th IAA/ASME/SAE/ASEE Joint Propulsion Conference & Exhibit 7-10 July 2002, Indianapolis, Indiana.
13. Bond, T.A., and Christensen, J.A., "NSTAR Ion Thrusters and Power Processors," NASA/CR 1999-209162, November 1999.
14. Patterson, M. J. and Benson, S. W., "NEXT Ion Propulsion System Development Status and Performance," AIAA-2007-5199, 43rd AIAA/ASME/SAE/ASEE Joint Propulsion Conference and Exhibit, Cincinnati, OH, July 8-11, 2007.
15. Polk, J.E., et al., "Performance and Wear Test Results for a 20-kW-Class Ion Engine with Carbon-Carbon Grids," AIAA 2005-4393, 41st AIAA/ASME/SAE/ASEE Joint Propulsion Conference & Exhibit, 10 - 13 July 2005, Tucson, Arizona.
16. Vaughan, C.E., Cassady, R.J. and Fisher, J.R., "The Design, Fabrication and Test of a 26-kW Arcjet and Power Conditioning Unit," IEPC-93-048, Seattle, WA, 1993.
17. Sutton, A.M., "Overview of the Air Force ESEX Flight Experiment," IEPC 93-057, Seattle, WA, 1993.
18. Frisbee, R., "Evaluation of High-Power Solar Electric Propulsion Using Advanced Ion, Hall, MPD, and PIT Thrusters for Lunar and Mars Cargo Missions," AIAA 2006-4465, 42nd AIAA/ASME/SAE/ASEE Joint Propulsion Conference & Exhibit, 2006, 10.2514/6.2006-4465.